

Research on Fracture Characteristics of Key Strata and Prevention of Mining-Induced Seismic Disasters in Kilometer-Deep Coal Mining

Xiaoming Sun ^{a, b, c}, Lei Wang ^{a, b, c}, Wenchao Zhao ^d, Yong Zhang ^{a, b, c}, Chengyu Miao ^{e*}

a. Inner Mongolia Research Institute, China University of Mining and Technology (Beijing), Ordos 017000, China

b. State Key Laboratory for Tunnel Engineering, China University of Mining and Technology (Beijing), Beijing 100083, China

c. School of Mechanics and Civil Engineering, China University of Mining and Technology (Beijing), Beijing 100083, China

d. College of Fire Protection Engineering, China People's Police University, Langfang 065000, China

e. School of Engineering and Technology, China University of Geosciences, Beijing 100083, China

*Corresponding Author: Chengyu Miao (CUMTB_MCY@163.com)

Abstract: Understanding the fracture characteristics of overlying key strata in goaf during coal mining and the mechanisms by which they induce seismic disasters is crucial for seismic disaster prevention and control. Using a mining-induced seismic event in the 0901 working face of the Daqiang Coal Mine as the research context, this paper conducts bottom unloading experiments on rock beams under dual-sided loading with varying rock beam thicknesses and unloading spans. These experiments simulate the dynamic phenomenon of key stratum rock beam fracture induced by sudden subsidence of lower strata during mining. Experimental results show that bottom unloading damage to all rock beams exhibits tensile-shear failure modes, accompanied by surface rock debris ejection as a dynamic failure phenomenon. Increasing rock beam thickness leads to a higher proportion of shear cracks and more severe surface dynamic failure phenomena. Conversely, increasing the unloading span results in a higher proportion of tensile cracks and the disappearance of the arched fracture zone. Combining stress path analysis and acoustic emission (AE) characteristics reveals that all rock beams experience multiple stress reduction phases during fracturing. The largest stress reduction occurs during the initial stress drop phase, preceding the appearance of peak energy dissipation. As the rock beam thickness and unloading span increase, the cumulative AE count, peak energy, and cumulative energy during unloading also increase, showing a certain degree of linearity. Based on the full-cycle failure mechanism of seismic impact on roadways, this study proposes a seismic disaster control mechanism and strategies based on the "dual compensation theory." Field applications demonstrate that the "dual compensation theory" and its associated control techniques effectively reduce the frequency and energy level of seismic events while significantly improving roadway stability during retreating operations.

Keyword: Key stratum fracture; Rock beam bottom unloading; Dual compensation theory; Mine seismic disaster

prevention

1. Introduction

As coal mining extends deeper underground, kilometer-deep mines are increasingly exposed to complex geomechanical environments, where mining-induced seismic disasters occur frequently. These disasters pose significant threats to mine safety and human lives ^[1-4]. The formation of seismic disasters is closely related to the fracture of overlying key strata, and with increasing mining depth and intensity, the stress environment and fracture characteristics of overlying strata in goaf become more complex, leading to higher frequencies and intensities of seismic events ^[5-7]. The dynamic disaster effects not only directly cause instability of roadway surrounding rock, failure of support structures, and other cascading damages, but also pose persistent threats to the dynamic safety of mine operations. Thus, systematically revealing the fracture characteristics of key strata and the mechanisms by which they induce seismic disasters is of great significance for effectively preventing seismic disasters and ensuring safe, efficient coal mining in deep mines.

In recent years, significant research has been conducted to ascertain the mechanisms of dynamic disasters in deep mines. Many scholars have focused on the fracture and movement laws of the roof strata in mining fields. Regarding physical and numerical experiments, Xiong et al. ^[8] used physical model tests and digital speckle techniques to study the movement laws of overlying strata in steeply inclined working faces and the length effect of working faces, finding that damage propagates along the "roof-overlying strata-roof" direction. Dai et al. ^[9] combined physical simulation experiments with the fractal dimension calculation of cracks, revealing the evolution characteristics of large spatial overlying strata cracks during the mining of thick, hard roof coal seams. Zhou et al. ^[10] developed numerical tools based on the material point method and strain-softening constitutive models to simulate the complex physical behavior of roof strata during mining. Numerical results indicate that cross joints and bedding planes significantly influence roof collapse. Liu et al. ^[11] established a 3D discrete element model of composite roof strata structures considering the influence of the hard rock proportion coefficient, analyzing crack evolution laws and distributions in overlying strata during different mining stages. Regarding theoretical analysis, Deng et al. ^[12] established a key stratum structural model to describe the intense dynamic behavior of roof strata during high-intensity mining under high-stress conditions, focusing on the fracture characteristics of ultra-thick coal seam roofs. Wu et al. ^[13] proposed a fracture structure model involving "cantilever beams-non-hinged roof-hinged roof combinations" for large mining height working faces and revised traditional roof collapse height calculation methods. Cheng et al. ^[14], using microseismic monitoring data, developed a movement zoning model of roof strata in vertical and horizontal directions. Despite these advances, systematic research on the fracture characteristics of key strata and the energy release laws of seismic events under deep mining conditions remains limited. In particular,

the effects of parameters such as rock beam thickness and unloading span on fracture modes and dynamic responses require further exploration. Moreover, current studies on the mechanisms by which key stratum fractures induce seismic events mainly focus on static mechanical analysis, leaving gaps in experimental reproduction of stress path evolution, crack propagation characteristics, and energy release laws during dynamic unloading.

Building on these experimental and theoretical studies, scholars have further developed control techniques for dynamic disasters and their derivatives. Li et al. ^[15] proposed six preventive measures to mitigate the disasters of fault-pillar-induced rock bursts (FPIRB) and found that stress-relief blasting and large-diameter drilling effectively reduce FPIRB occurrences. Ning et al. ^[16] conducted field studies on the fracture and movement characteristics of dual-layer hard thick rock strata under longwall top coal caving conditions, subsequently proposing long-hole pre-splitting blasting techniques to weaken the strength and mass of dual-layer hard roofs. Li et al. ^[17] addressed asymmetric large deformation disasters caused by intense dynamic loads from hard roofs in gob-side roadways by proposing a combined control method involving roadway widening, long-anchor cable installation, and blasting roof cutting. Kuang et al. ^[18], based on in-situ exploration techniques, established the spatiotemporal correspondence between key stratum fractures, movement, and rock bursts, employing hydraulic fracturing and deep-hole blasting to weaken energy release during rock bursts. Current studies suggest that most traditional seismic disaster control measures focus on passive prevention during individual stages, lacking proactive control strategies spanning the entire cycle, from roadway excavation to seismic impact. Optimizing support structures and mining processes to achieve controllable energy release from key stratum fractures and synergistic stability control of surrounding rock remains a core challenge in safe, efficient deep mining.

Using the seismic events in the 0901 working face of the Daqiang Coal Mine as an engineering background, this study conducts bottom unloading experiments on rock beams with varying thicknesses and unloading spans to reveal the stress path evolution, crack propagation characteristics, and AE energy release laws during key stratum fracture. Based on the full-cycle failure mechanism of seismic impacts on roadways, this paper proposes the "dual compensation theory," integrating "excavation stress compensation" and "mining space compensation." Field applications of high-prestress NPR anchor cable support technology and double-sided roof cutting and unloading techniques validate the theory's effectiveness in reducing seismic event energy and frequency while improving roadway stability. These findings provide new theoretical and technical pathways for seismic disaster control in deep mines.

2. Engineering background

2.1 Mine overview

This study uses the 0901 working face of the Daqiang Coal Mine as the research context. Located in Shenyang, Liaoning Province, China (Figure 1a), the 0901 working face is the first mining face in the Daqiang Coal Mine. The inclined length of the 0901 working face is 241 m, its strike length is 1170 m, and its burial depth ranges from 1018 m to 1242 m. The 9# coal seam is mined, with an average dip angle of approximately 10° and an average thickness of 9.5 m, classifying it as an ultra-thick coal seam. Mining employs the inclined longwall mining method with a fully mechanized top coal caving technique, and roof management adopts the natural caving method. After mining, the maximum height of the caving zone is 36.4 m, while the maximum crack development height is 122.8 m.

During the retreat of the 0901 working face, three seismic events occurred, with magnitudes of 3.1, 3.3, and 2.9, releasing approximately 4.2×10^6 J, 9.0×10^6 J, and 1.2×10^6 J of energy, respectively. On-site microseismic monitoring preliminarily identified the three seismic events as being related to the fracture of overlying key strata in the mining field. Following the seismic events, the retreat roadway experienced severe deformation and damage, including overall cross-sectional shrinkage, roof subsidence, anchor cable breakage, steel arch distortion, and crossbeam bending (Figure 1b).

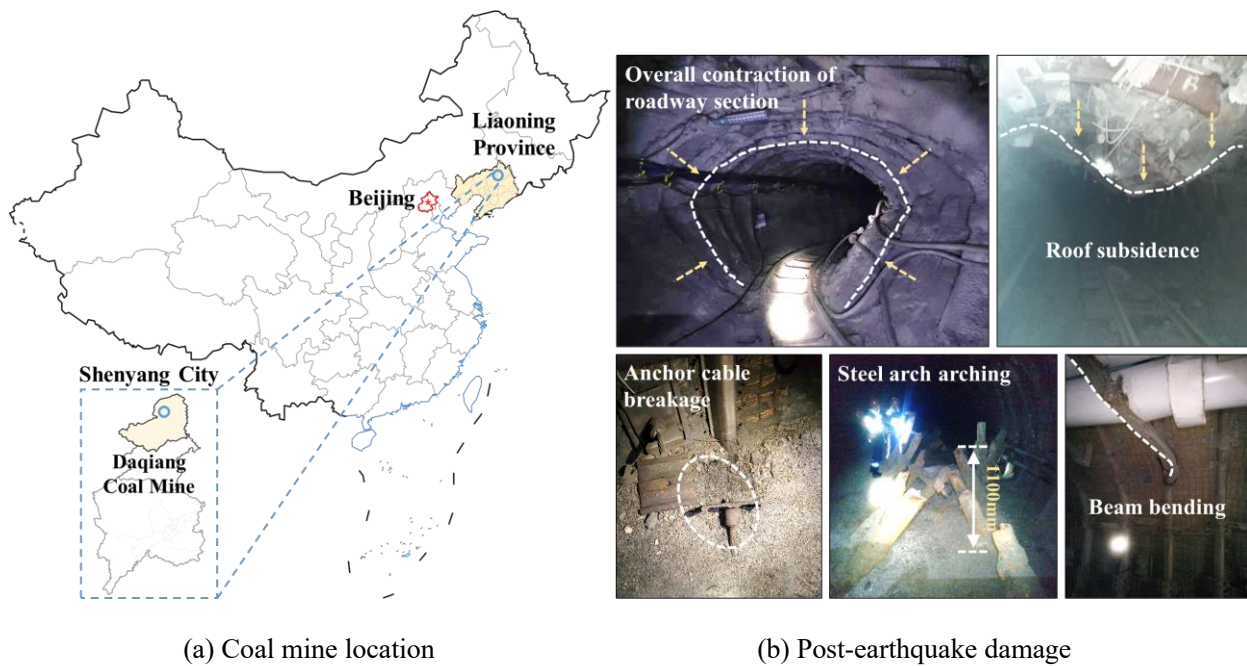


Figure 1 Basic overview of Daqiang coal mine

2.2 Key stratum identification

The primary cause of seismic events in the 0901 working face is the fracture of overlying key strata, making the determination of key stratum positions a prerequisite for laboratory experiments. Using the key stratum identification method^[19], three key strata positions in the overlying strata of the 0901 working face were

preliminarily identified. The results show that within 60 m above the roof of the working face, the first key stratum is primarily composed of a major roof rock beam; within the 60–100 m range, the second key stratum consists of a composite rock beam; and within the 100–150 m range, the third key stratum is a composite rock beam directly associated with seismic events.

Based on the vertical levels of seismic events in the 0901 working face, all three events occurred within the 120–150 m range. Within this range, there are hard rock layers of fine sandstone and medium sandstone, and the deformation energy released by the fracture of the composite rock beam in this range is the primary source of seismic energy. Therefore, this composite rock beam can be considered the key stratum directly inducing seismic events (referred to as the far-field key stratum). The fracture of the lower mudstone and medium sandstone-fine sandstone rock beams (near-field key strata) induces fractures in the overlying strata and the upper key stratum, acting as the first cause of seismic events. Based on the above analysis, the stratigraphic distribution of key strata in the 0901 working face overlying strata is shown in Figure 2.

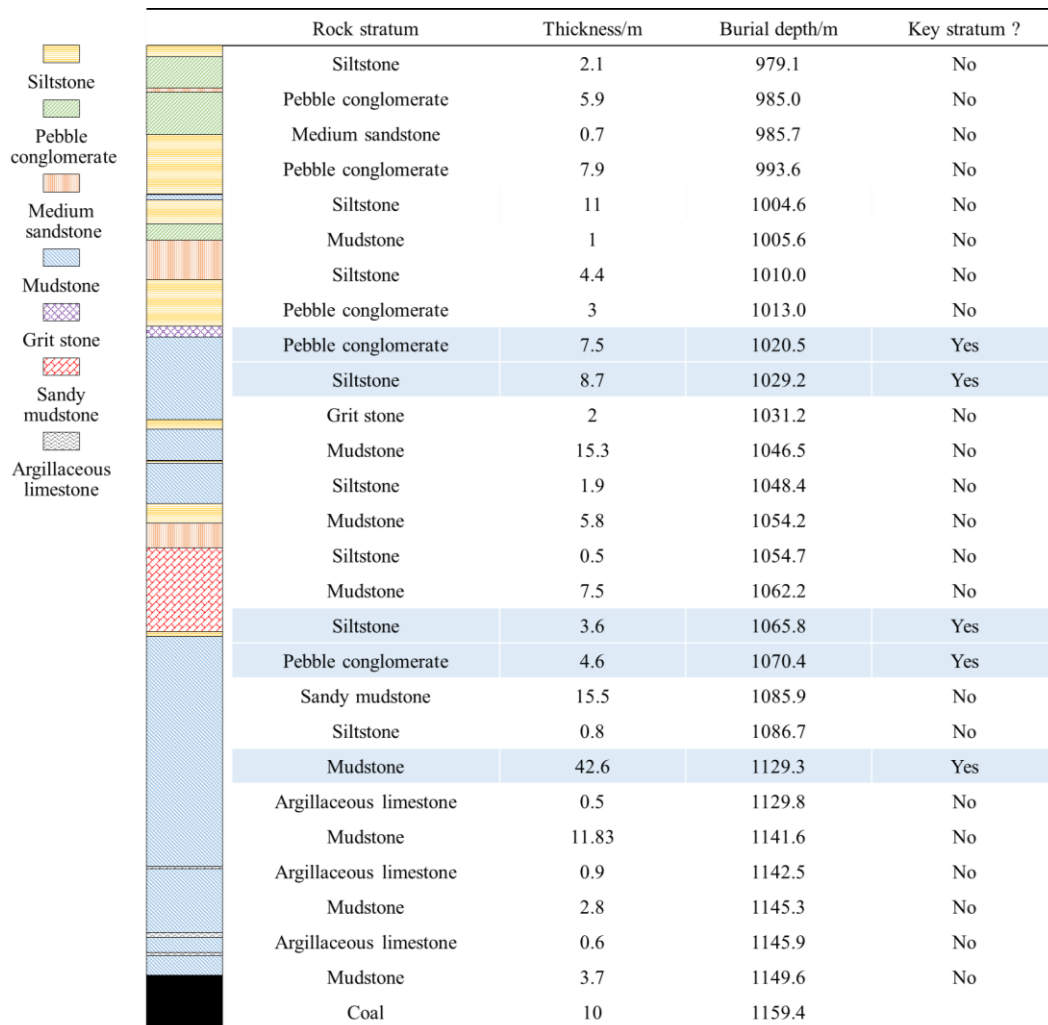


Figure 2 Determination results of key strata

3. Fracture characteristics of key stratum rock beams

3.1 Experimental scheme

Before mining, the key stratum and surrounding strata are under a three-dimensional stress environment. As the working face advances, the roof of the goaf continuously collapses. This deformation and damage propagate upward, causing the key stratum to bend and subside. The delamination formed between different strata provides space for key stratum fracturing, while the delamination also alters the stress environment, resulting in sudden unloading at the bottom of the stratum. To study the fracture characteristics of key strata under confining pressure and reproduce the dynamic phenomena of seismic events induced by key stratum fractures, bottom unloading experiments were conducted in the laboratory. Figure 3 demonstrates the three-dimensional stress changes of roof rock beams before and after mining. Before mining, roof rock beams are in a three-dimensional stress state (Figure 3(a)). After mining, the fractures and subsidence of shallow strata create a free surface for the upper rock beams. Stress perpendicular to the free surface becomes zero, and the rock beams transition from a three-dimensional six-sided loading state to a five-sided loading state with a free bottom surface. Assuming that the working face dimensions before the initial weighting of the major roof satisfy the ratio of the advancement distance aa to the working face length bb being less than 1 ($a/b < 1$), the rock beams before fracturing can be regarded as fixed beams at both ends^[20]. This condition is simplified as a four-sided loading and bottom unloading stress environment (Figure 3(b)). To simulate the phenomenon of lower strata subsiding suddenly during deep mining, causing rock beam fractures, the bottom unloading experiment adopts a "pre-stress environment—load holding—unloading" loading path. The specific stress path of the bottom unloading experiment is shown in Figure 3(c).

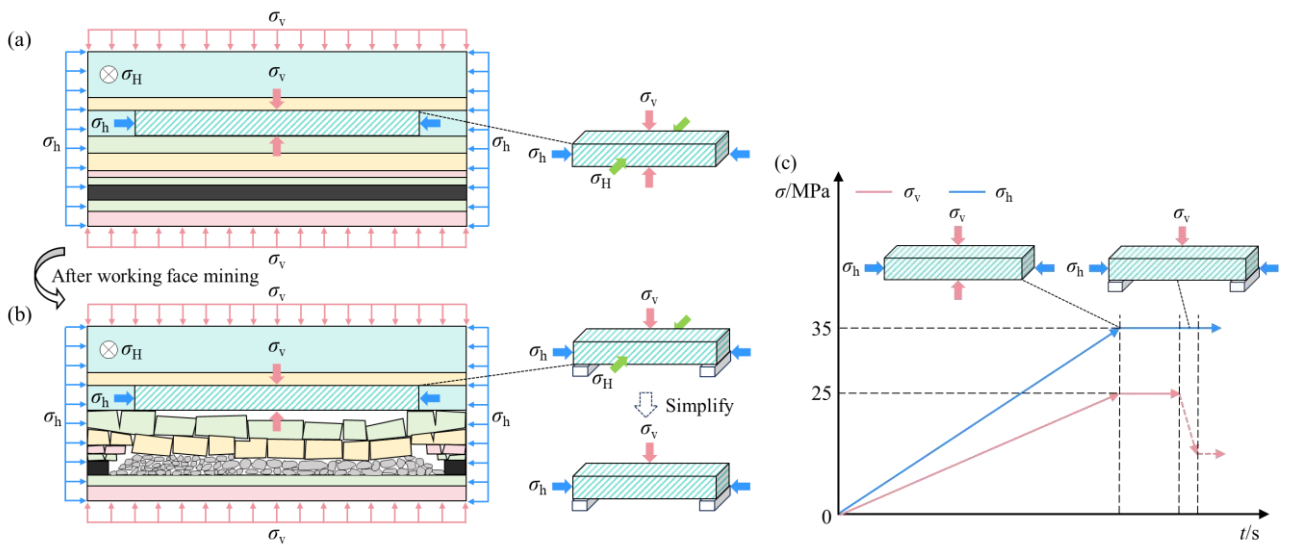
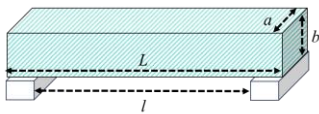


Figure 3 Three-dimensional stress variation of rock beam and experimental stress path

To investigate the effects of different rock beam thicknesses and unloading spans on fracture characteristics, fine sandstone samples were prepared based on the seismic source layer in the 0901 working face. Samples were

processed into uniform widths of 50 mm, with thicknesses of 30 mm, 40 mm, and 50 mm (lengths of 190 mm) and lengths of 140 mm, 190 mm, and 240 mm (thicknesses of 40 mm), totaling five samples. The parameters and distribution of the samples are shown in Table 1. The loading system for the experiment is a 2000 kN rock testing system, and the unloading system for confining pressure is a self-designed dual-directional loading single-sided unloading device, as shown in Figure 4(a). The device comprises sliding bearing bases, loading steel blocks, lateral steel plates, reaction steel plates, sliding bolt-nut kits, column jacks, and annular jacks. Based on measured in-situ stress data, the axial confining pressure was set to 25 MPa, and the horizontal confining pressure was set to 35 MPa, with a loading rate of 4 MPa/min. Once the confining pressure reached the design value, it was held constant. During the loading process, acoustic emission systems and high-speed cameras were used to monitor the internal acoustic emission signals and surface crack evolution characteristics of the samples in real time. The experimental setup and monitoring systems are shown in Figure 4(b).

Table 1 Basic parameters of rock beam samples

Basic parameters	Experiment factor	Width a/mm	Length L/mm	Thickness b/mm	Unloading span l/mm
 UCS: 78.01 MPa Elastic modulus: 9.20 GPa Poisson's ratio: 0.19	Specimen thickness	50	190	30 40 50	150
	Unloading span	50	140	40	100
			190		150
			240		200

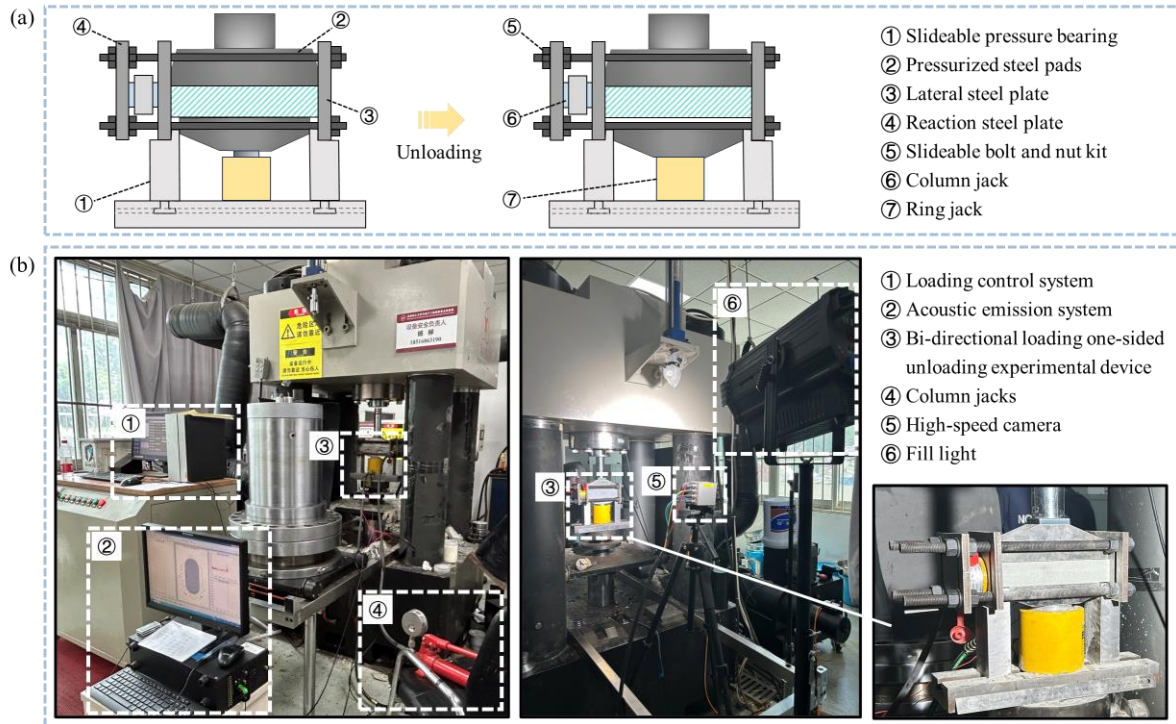


Figure 4 Unloading experimental system for the bottom of the rock beam

3.2 Deformation and damage evolution characteristics

Figure 5 shows the stress-time curves and crack evolution characteristics of rock beams with different thicknesses and unloading spans. During the deformation and damage process, all samples experienced four stages: compaction, elastic deformation, load-holding stability, and fracture failure. As shown in the figure, the stress paths of rock beams with different thicknesses and spans exhibit similar trends. When the load reaches the initial target stress, the rock beams remain stable and intact, with no significant cracks. Upon bottom unloading, the vertical stress rapidly decreases, leading to rapid expansion in the unloading direction, and the rock beams quickly develop numerous cracks within a short period. From the bottom unloading stage to the final failure stage, multiple stress reduction phenomena occur, ultimately causing significant fractures.

Under an unloading span of 150 mm, the crack evolution characteristics during the unloading process for rock beams of different thicknesses are shown in Figure 5(a). After unloading, a few tensile cracks first appear in the middle or at both ends of the rock beams. As loading continues, tensile cracks expand toward the top of the rock beam, forming shear cracks. Simultaneously, due to the horizontal confining pressure, some shear cracks propagate from both ends of the rock beam toward the center. Ultimately, the cracks are distributed in an arch-shaped pattern, accompanied by surface rock debris ejection as a dynamic failure phenomenon. Comparing the final failure morphologies of the rock beams, it is observed that as rock beam thickness increases, the proportion of tensile cracks decreases, while shear cracks increase, and surface dynamic failure phenomena become more severe. This is primarily because the increased thickness reduces the flexural deformation capacity of the rock beam, causing energy to be released more as fracture energy rather than through flexural deformation during unloading.

For rock beams with a thickness of 40 mm, the crack evolution characteristics during the unloading process for different spans are shown in Figure 5(b). After unloading, the cracks in all rock beams exhibit tensile-shear failure modes. Comparing the final failure morphologies of the rock beams, it is observed that as unloading spans increase, the proportion of tensile cracks rises, shear cracks decrease, and the arched crack zone gradually disappears. During the unloading failure of all rock beams, surface rock debris ejection as a dynamic failure phenomenon occurs, primarily at the contact points between the rock beam ends and the supports. This is due to stress concentration in these areas, where deformation energy is relatively high, leading to a sudden release of stress during unloading.

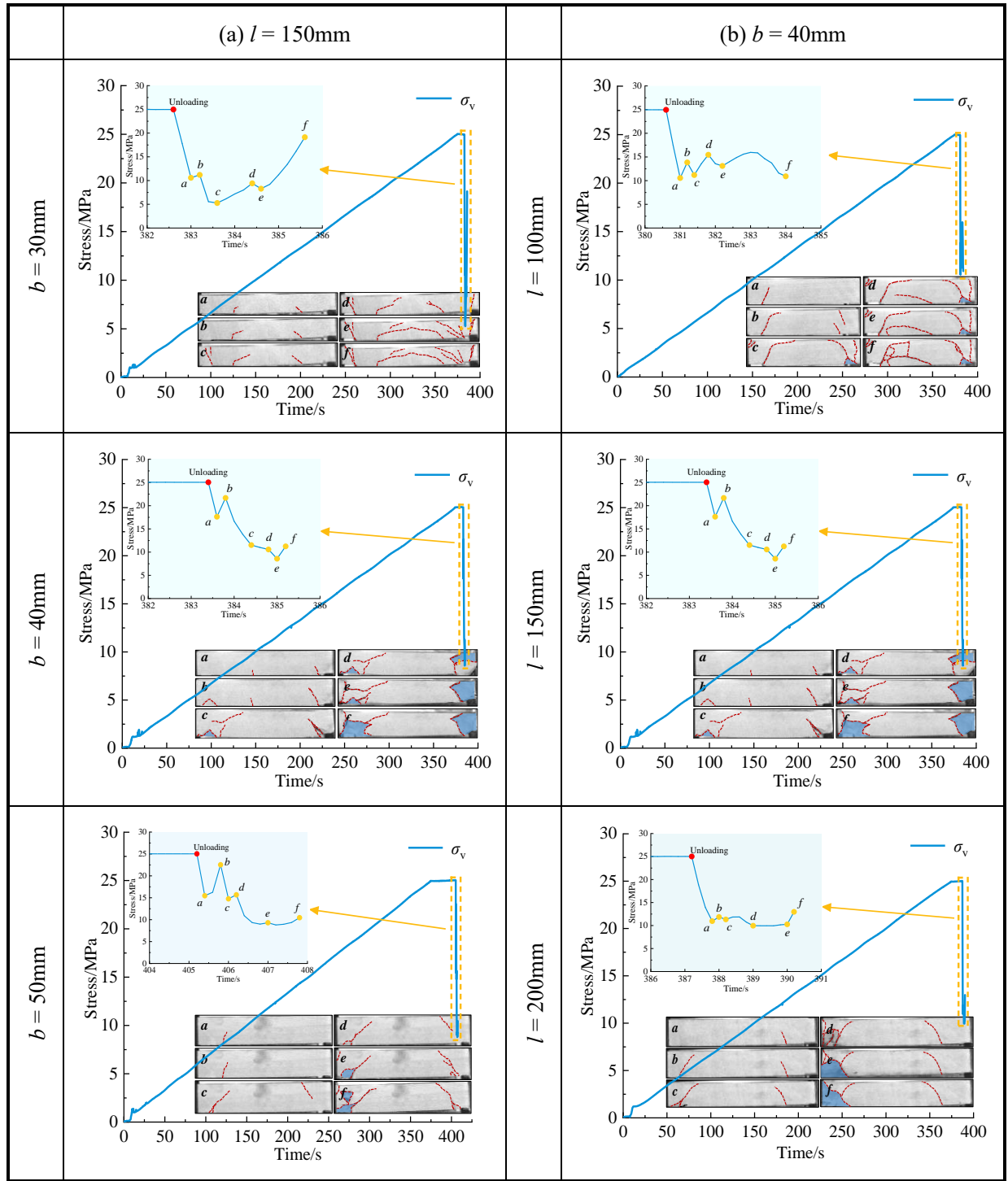


Figure 5 Stress-time curve and fracture evolution characteristics of the rock beam

3.3 Acoustic emission evolution characteristics

Figure 6 presents the acoustic emission (AE) evolution characteristics of rock beams with varying thicknesses and unloading spans. It is observed that during the compaction and elastic deformation stages, the AE count and AE energy of all rock beams remain at low levels. During these stages, the primary cracks within the rock beams close due to applied stress, resulting in relatively low and evenly distributed AE signals. When the applied stress reaches the design value and stabilizes, the AE signals essentially disappear, indicating that the development of internal cracks within the rock beams is relatively stable during this stage. Once bottom unloading begins, the stress on the

bottom surface instantly disappears, causing pre-existing cracks within the rock beams to rapidly expand and develop, accompanied by surface rock ejection. At this point, AE counts exhibit a sudden burst, energy values increase significantly, and cumulative energy reaches its peak in a short time.

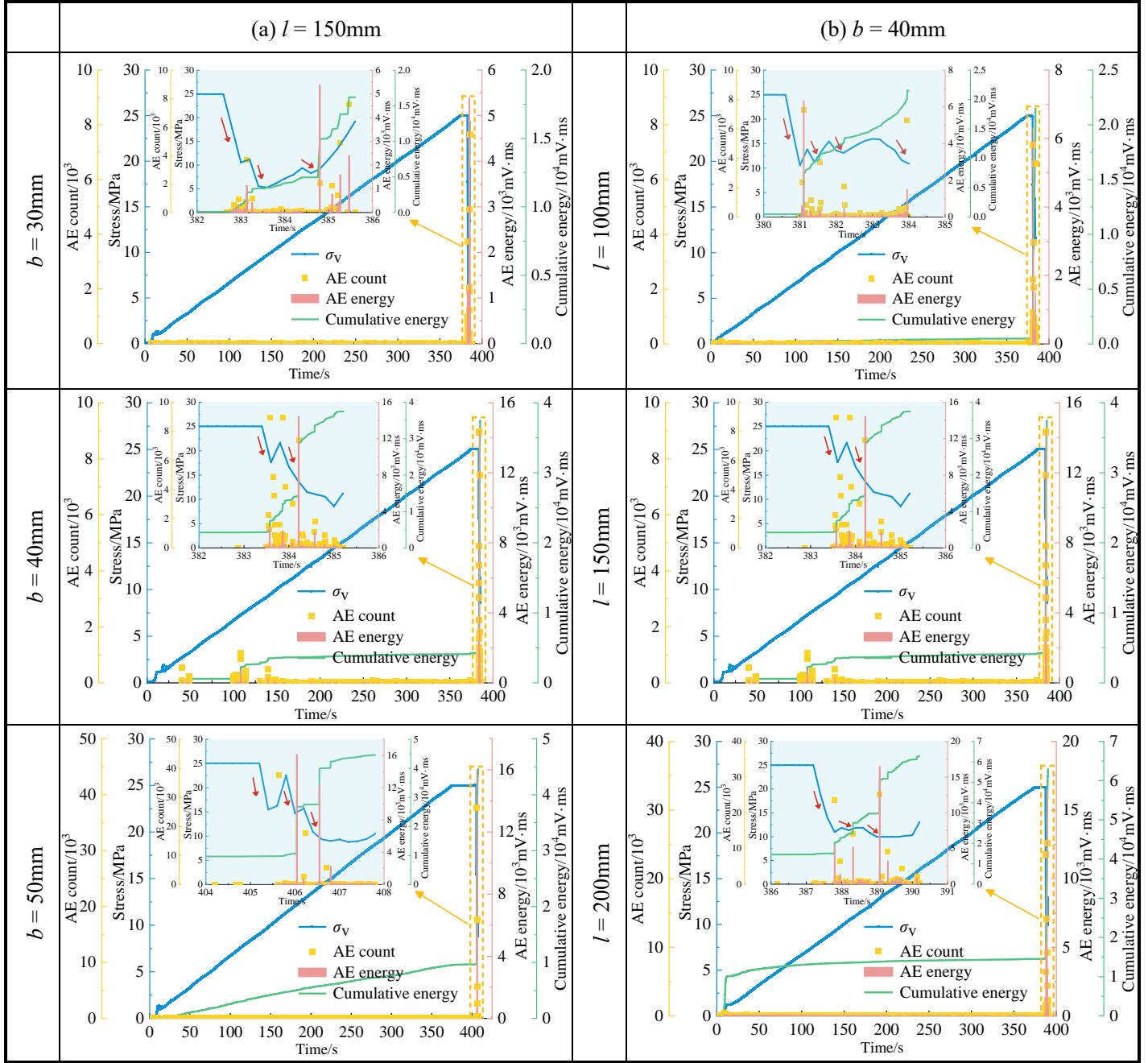


Figure 6 Acoustic emission evolution characteristics of the rock beam

By correlating the stress-time curves during unloading with AE evolution characteristics, the relationship between axial stress variations and AE peak energy, or large energy events, is further investigated. Under an unloading span of 150 mm and rock beam thicknesses of 30 mm, 40 mm, and 50 mm, 3, 2, and 3 occurrences of stress reduction phenomena are observed, respectively, during the bottom unloading process. The initial stress reduction amplitudes are 14.41 MPa, 7.38 MPa, and 9.54 MPa, and the time of the initial stress reduction precedes the occurrence of the peak energy dissipation by 2.20 s, 0.81 s, and 0.84 s, respectively. For a rock beam thickness

of 40 mm and unloading spans of 100 mm, 150 mm, and 200 mm, 4, 2, and 3 occurrences of stress reduction phenomena are observed, respectively. The initial stress reduction amplitudes are 14.44 MPa, 7.38 MPa, and 14.04 MPa, and the initial stress reduction times precede the peak energy dissipation times by 0.50 s, 0.81 s, and 1.88 s, respectively. Comprehensive analysis reveals that during the fracturing process, all rock beams experience 2 to 4 occurrences of stress reduction phenomena. The largest stress reduction amplitude usually occurs during the initial stress reduction phase. Additionally, it is found that the occurrence of stress reduction phenomena precedes the occurrence of peak energy dissipation in all cases. In other words, stress reduction phenomena are precursors to large energy dissipation events.

To further examine the relationship between AE characteristics during unloading and the rock beam thickness and unloading span, the cumulative AE count, peak energy, and cumulative energy during unloading are analyzed. Scatter plots of AE characteristic values versus thickness and span are generated, and linear fitting is performed for each group of data. Figure 7(a) illustrates the relationship between AE characteristic values and rock beam thickness during unloading. The fitted curves indicate that all AE characteristic values exhibit a certain linear relationship with rock beam thickness; specifically, the cumulative AE count, peak energy, and cumulative energy increase with increasing rock beam thickness. This is because the increase in rock beam thickness leads to higher elastic energy storage within the rock beams, resulting in higher energy levels during fracturing. From an engineering perspective, reducing the thickness of overlying strata in mining fields with ultra-thick rock layers can decrease the frequency and energy levels of large energy events.

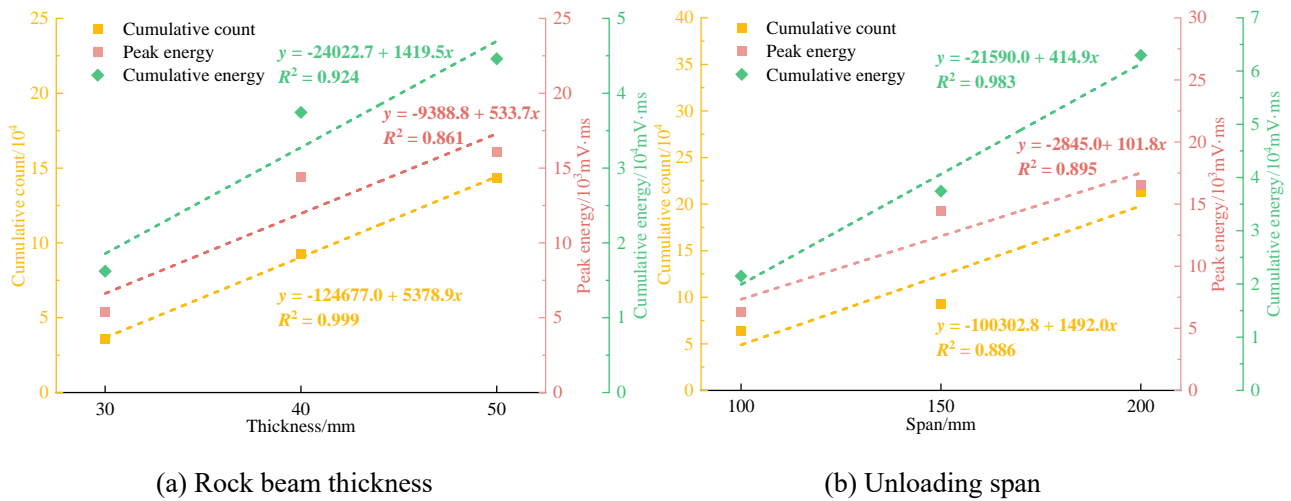


Figure 7 Relationship between acoustic emission characteristics and rock beam thickness/unloading span

Figure 7(b) illustrates the relationship between AE characteristic values and unloading span during unloading. The cumulative AE count, peak energy, and cumulative energy during unloading increase with increasing unloading span, also showing a certain degree of linearity. This observation aligns with the patterns of microseismic monitoring signals during mining operations, where the width and extent of roof delamination increase with the working face

span, leading to frequent bursts of microseismic signals and large energy events. From an engineering perspective, controlling the development of roof delamination by reducing the unloading range can effectively reduce the frequency and energy levels of microseismic events.

4. Mechanism of seismic disaster prevention for key stratum fractures

4.1 Full-cycle failure mechanism of seismic impact on roadways

Seismic events typically occur during the full mining stage of the working face, and their disaster-inducing effects on roadways are also generated during this period. At this time, the stability of roadway surrounding rock is successively affected by three disaster-causing factors: roadway excavation, working face mining, and seismic impacts. Therefore, addressing the deformation disasters of roadway surrounding rock caused by seismic impacts cannot be limited to the seismic event occurrence stage alone. Rather, such efforts should begin during the roadway excavation stage, with proactive prevention and step-by-step measures. In this paper, the stress states of roadway surrounding rock are divided into three stages, from excavation formation to the influence of seismic events:

Stage 1: Roadway excavation stage. From the perspective of Mohr's circle and the Mohr-Coulomb envelope, the effects of excavation on the stability of roadway surrounding rock are analyzed, as shown in Figure 8(a). After excavation, the stress state of the surrounding rock near the free surface undergoes two changes: (1) radial stress σ_3 of the surrounding rock becomes zero, and (2) circumferential stress increases nearly twofold due to stress concentration caused by excavation ^[21]. These effects result in instability and failure of the surrounding rock. If initial support is applied promptly and with sufficient strength, the failure can be mitigated but not fundamentally resolved.

Stage 2: Working face mining stage. After initial support, the surrounding rock of the roadway achieves a relatively stable state. However, during mining, the periodic fracture of the roof strata in the mined-out area causes the surrounding rock to experience multiple disturbances from superimposed stresses. Particularly in ultra-thick coal seams, the large rotational subsidence space of the roof and intense fracturing activity lead to greater stress concentration in the roadway, as shown in Figure 8(b). The stress concentration ($\sigma_{(i-s)}$) increases several times, causing severe deformation and failure of the initially stabilized roadway, necessitating reinforcement and strengthening of the original support.

Stage 3: Seismic Event Stage. During seismic events, the far-field key stratum fractures and releases stored elastic energy instantaneously. The impact energy rapidly transmits to the roadway's surrounding rock and support structures, significantly expanding the plastic zone of the surrounding rock. If the support structure cannot absorb this sudden impact energy, changes in the stress state of the surrounding rock will alter the roadway's spatial state, leading to severe instability and failure. As shown in Figure 8(c), the surrounding rock, after experiencing

excavation and mining disturbances, achieves a quasi-stable state with multiple reinforcement measures. However, when seismic energy is transmitted from the fractured key stratum to the surrounding rock and support structure, the reinforcement measures fail completely, resulting in intense impact-induced failure of the roadway.

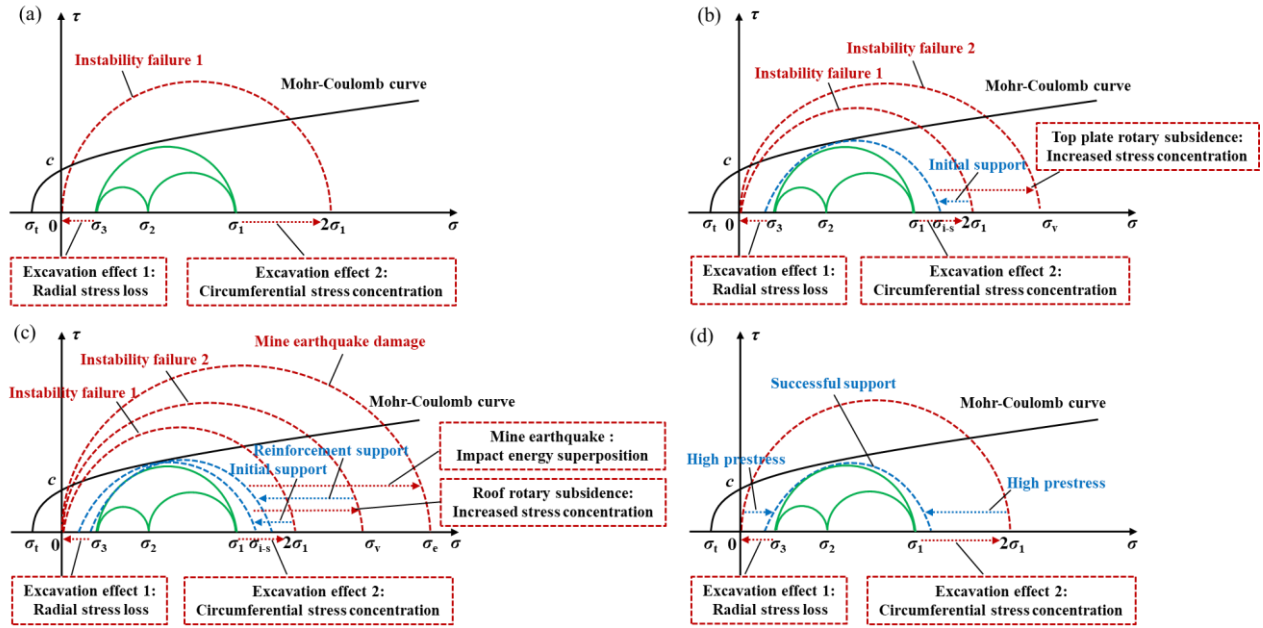


Figure 8 Stress state evolution of surrounding rock in mining-induced impact roadways

4.2 Seismic disaster control mechanism based on the "dual compensation theory"

The prevention or mitigation of dynamic disasters caused by key stratum fractures primarily involves two approaches: (1) shortening the transition time between pre- and post-excavation or mining static systems to ensure predictability, and (2) reducing the activity intensity of individual stratum units during the transition to lower disaster intensity. Thus, the root cause of seismic disasters lies in roadway excavation and coal seam mining, and the key to resolving dynamic disaster problems is effective excavation compensation and mining compensation. The core of the "dual compensation theory" is to reduce the activity intensity of individual stratum units during each phase.

4.2.1 Excavation compensation mechanism

Based on the three-stage stress state analysis of roadway surrounding rock, the fundamental cause of instability is the lack of timely high-stress compensation for the excavated surrounding rock and insufficient energy absorption by support structures. To address this issue, a control method involving "high-prestress compensation + NPR (Negative Poisson's Ratio) constant-resistance support" is proposed. After excavation, high-prestress NPR anchor cables are applied to the shallow surrounding rock, restoring it from a two-dimensional stress state to a three-dimensional one. As the minimum principal stress of the shallow surrounding rock increases, the degree of stress concentration decreases accordingly, as shown in Figure 8(d). During the mining and seismic impact stages, the surrounding rock with high-stress compensation maintains a relatively stable stress environment without significant

stress reduction. Additionally, the constant-resistance large-deformation effect of NPR anchor cables efficiently absorbs impact energy through relative sliding between the constant-resistance sleeve and the cone^[22,23]. As a result, the NPR-supported surrounding rock maintains its load-bearing capacity, ensuring overall stability.

4.2.2 Mining compensation mechanism

Under conventional 121 mining methods, the overlying strata in the mined-out area experience damage in three zones: caving zone, fracture zone, and sagging zone. Seismic events predominantly occur within the fracture zone, as shown in Figure 9(a). Mining compensation involves pre-splitting the roof on both sides of the working face^[24], increasing the caving zone height to allow sufficient caving and bulking of the overlying strata, thereby compensating for mining-induced spatial loss. The collapsed strata support the high-level roof, restricting deformation and fracture of key strata that could induce seismic events, as shown in Figure 9(b). By controlling roof fracturing, mining-induced pressure is correspondingly reduced. Thus, mining compensation effectively controls seismic disasters by compensating for spatial losses and reducing disturbance intensity.

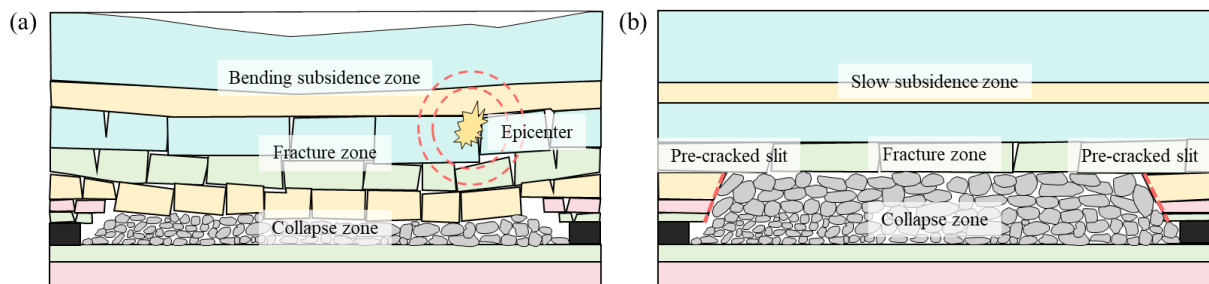


Figure 9 Comparison of roof collapse characteristics

5. Control strategies for key stratum fracture-induced seismic events

5.1 Overall control approach

Based on the research above, this study selects the 0908 working face of the Daqiang Coal Mine as a field experiment site to validate the effectiveness of the "dual compensation theory" for preventing key stratum fracture-induced seismic events. The 0908 working face is the adjacent working face to the 0901 working face, separated by a coal pillar of 50 m. During the mining of the 0901 working face, three seismic events occurred, severely affecting the safety of mining operations. Due to the proximity of the 0908 working face, its overlying roof lithology and structure are similar to those of the 0901 working face, with the same seismic event-inducing key strata. Therefore, during the mining of the 0908 working face, seismic events are likely to occur due to the influence of the mined-out area of the 0901 working face.

To prevent seismic events and maintain roadway stability in the 0908 working face, this study applies dual-sided roof cutting and unloading techniques^[25,26] and high-prestress NPR anchor cable support technology^[27,28], based on the mechanisms of excavation compensation and mining compensation in the "dual compensation theory."

The control strategy integrates roof cutting and support, with an overall layout of three grades of roof cutting: deep and shallow hole combined roof cutting on both sides of the roadway, roof cutting for crossheadings and retreat channels, and stepwise roof cutting along the working face. At the same time, high-prestress NPR anchor cables are applied to support the roadways, crossheadings, and retreat channels. The specific layout and key parameters of pre-splitting roof cutting and anchor cable support are shown in Figure 10.

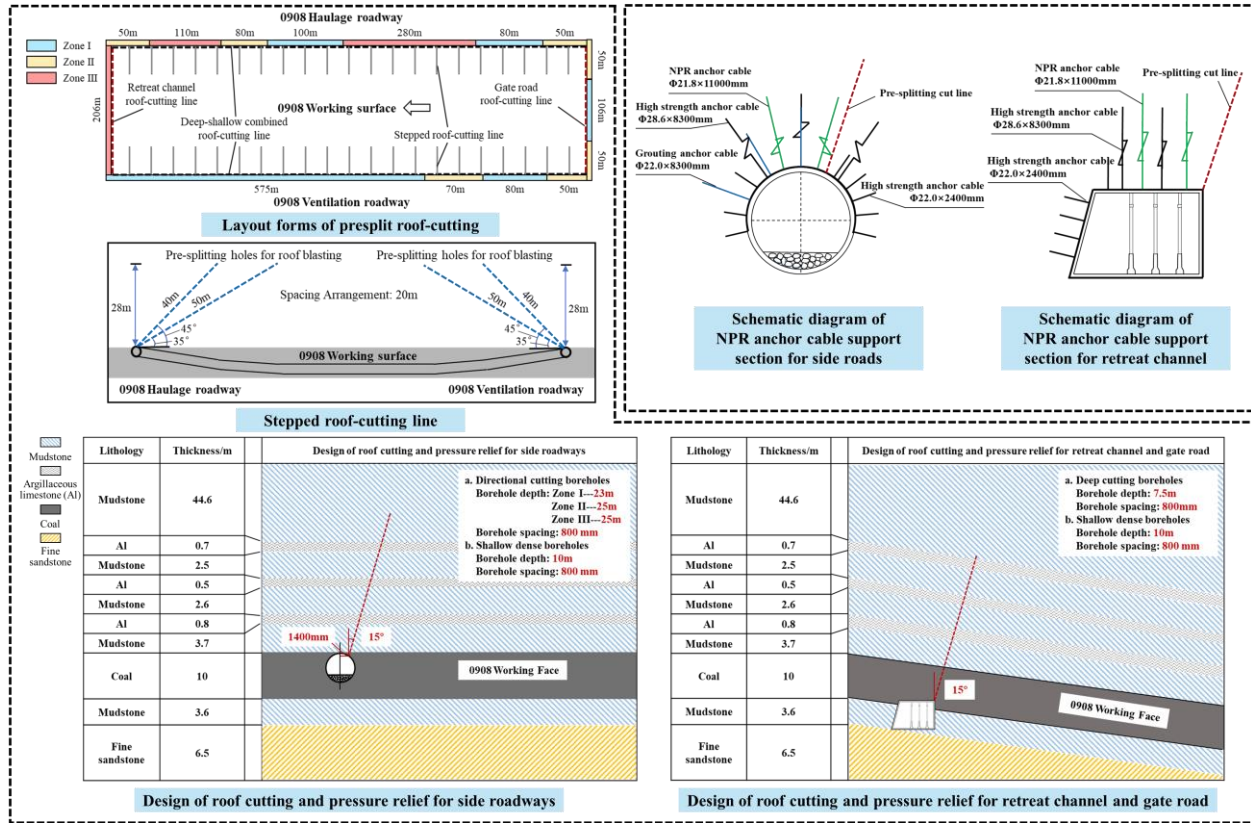


Figure 10 Layout forms and key parameters of pre-splitting roof cutting and anchor cable support

5.2 Field control results

5.2.1 Microseismic monitoring

The monitoring system was deployed along the mining roadway of the 0908 working face, with two monitoring stations located 275 m and 475 m away from the crossheading. Each station included monitoring points for NPR anchor cable force and deformation, as well as roadway surface displacement. Combined with the existing microseismic monitoring system, a comprehensive seismic monitoring network was established.

Statistical analysis of microseismic data during the mining of the 0908 working face revealed that the energy levels of microseismic events were generally below 10^5 J. At approximately 221 m and 420 m of mining progress, two relatively large energy microseismic events occurred, with energy levels of 1.32×10^6 J and 1.73×10^6 J, respectively. Among all microseismic events, 21.89% had energy levels below 10^2 J, 62.66% were between 10^2 J and 10^3 J, 15.36% were between 10^3 J and 10^4 J, and 0.09% were between 10^4 J and 10^5 J. By projecting the three-dimensional coordinates of microseismic event sources onto the layout of the working face, horizontal and vertical

projections of the event sources were obtained, as shown in Figure 11(a). The projection results indicate that approximately 65% of the event sources are located on the side of the 0901 mined-out area, influenced by the adjacent mining of the 0901 working face. Microseismic events primarily occurred within 50 m above the coal seam roof in mudstone layers and within 10 m below the coal seam floor in sandstone layers. Large energy events occurred within the range of approximately 100–110 m above the roof.

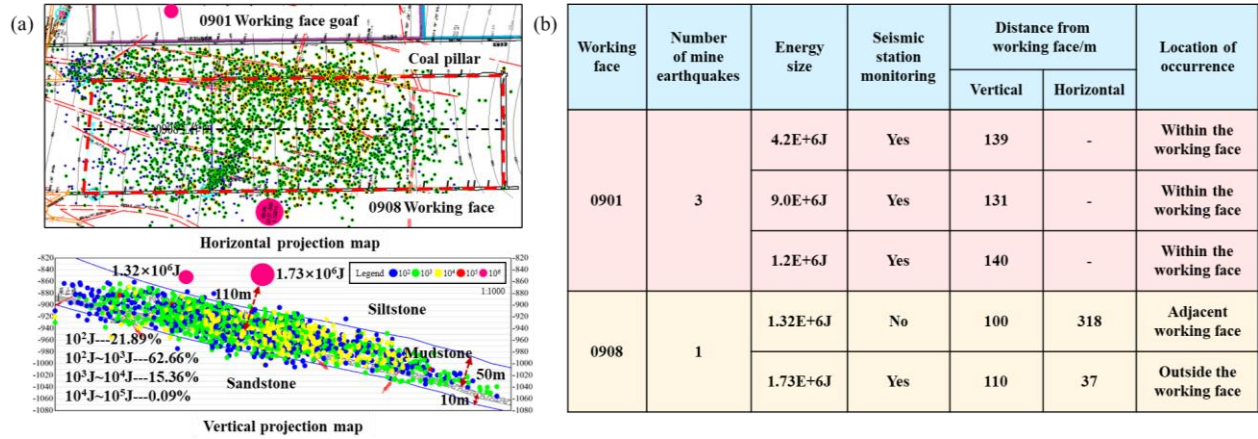


Figure 11 Microseismic monitoring data of 0908 working face

A comparison of seismic data from the 0908 and 0901 working faces is shown in Figure 11(b). After applying mining compensation, the frequency and energy levels of large energy events during the mining of the 0908 working face decreased, and the height of roof fracture development was reduced. Additionally, large energy events were relocated to areas outside the mining compensation zone. This indicates that the mining compensation technology effectively blocked the transmission of roof stress, causing the overlying strata above the mined-out area to collapse fully within the pre-split roof cutting height. The collapsed strata filled and supported the overlying strata, reducing roof movement intensity and fracture activity.

5.2.2 Monitoring of NPR anchor cable axial force and deformation

Figure 12 shows the monitoring curves of NPR anchor cable axial force and deformation during the mining of the 0908 working face. When the working face advanced to approximately 50 m from monitoring stations #1 and #2, the axial force of the anchor cables began to increase rapidly. As the working face advanced to approximately 25 m from the monitoring stations, corresponding to mining progress of 221 m and 420 m, the first large energy microseismic event and the largest energy microseismic event during the mining period occurred. At this point, the NPR anchor cables at stations #1 and #2 entered the constant-resistance stage, with relative sliding between the cone and sleeve of the anchor cables. The initial deformation reached 18 mm and 38 mm, respectively. As mining continued, the axial force of the NPR anchor cables fluctuated around the constant-resistance value, and the final deformation increased rapidly to 80 mm and 86 mm, respectively. At this stage, the impact energy transmitted from the fractured overlying strata to the surrounding rock of the roadway was continuously absorbed, and the NPR

anchor cables maintained effective control.

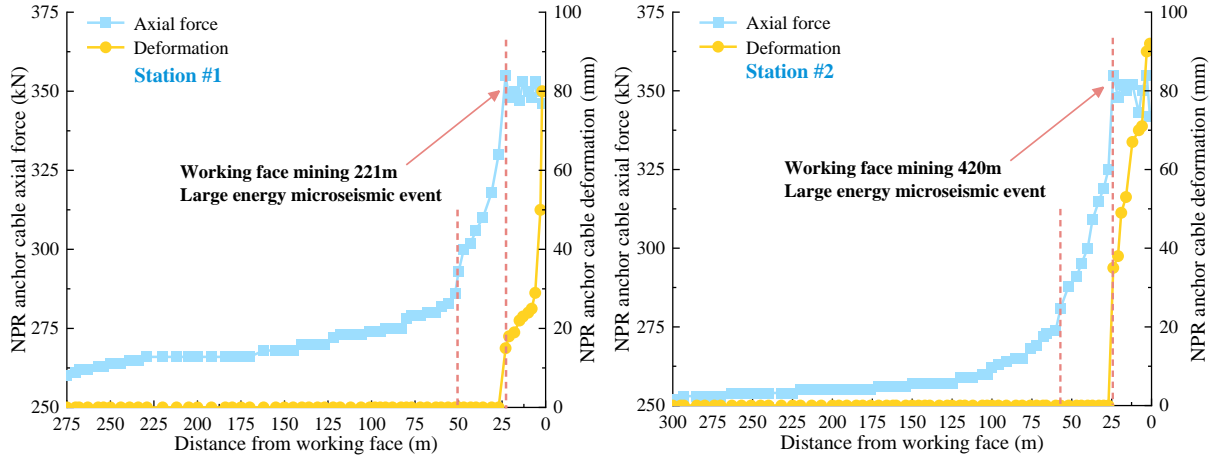


Figure 12 Monitoring of NPR cable axial force and deformation

5.2.3 Monitoring of surrounding rock displacement

Figure 13 shows the monitoring curves of surrounding rock displacement during the mining of the 0908 working face. The cumulative convergence of the roof and floor in the transport roadway and return airway of the 0908 working face was controlled within 400 mm and 300 mm, respectively, while the sidewall convergence was controlled within 300 mm and 230 mm, respectively. Compared with the 0901 working face, the displacement was reduced by approximately 50% and 75% in the two roadways, respectively. Furthermore, during the two large-energy microseismic events, the surrounding rock of the two roadways showed no significant deformation and remained stable.

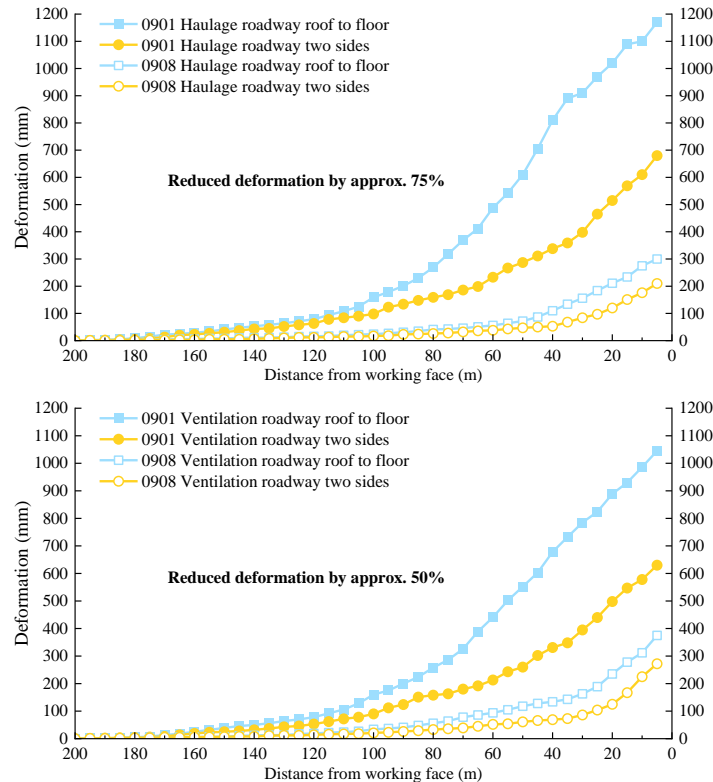


Figure 13 Monitoring of surrounding rock deformation

Finally, based on the "dual compensation theory," the application of dual-sided roof cutting and unloading techniques and high-prestress NPR anchor cable support technology resulted in a satisfactory field control effect, as shown in Figure 14. During the mining of the 0908 working face, the two roadways remained stable, and mining operations were conducted safely and continuously. The excellent application results demonstrate that the "dual compensation theory" and its associated control technologies effectively prevent key stratum fracture-induced seismic events.

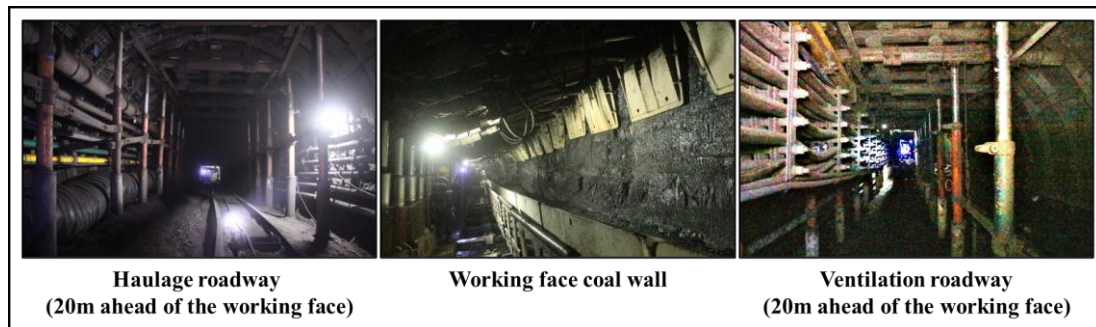


Figure 14 Field control effect

6. Conclusions

- (1) After bottom unloading, all rock beams exhibited tensile-shear failure modes, accompanied by surface rock debris ejection as a dynamic failure phenomenon. Rock beam thickness and unloading span significantly influenced the fracture characteristics under bottom unloading conditions. With increasing thickness, the proportion of shear cracks increased, and surface dynamic failure became more severe. Conversely, with increasing unloading span, the proportion of tensile cracks increased, and the arched fracture zone disappeared.
- (2) During the fracturing process, all rock beams experienced 2 to 4 stress reduction phenomena, with the largest stress reduction amplitude typically occurring in the initial stress reduction phase. Additionally, stress reduction phenomena always preceded the occurrence of peak energy dissipation, indicating that stress reduction is a precursor to large energy dissipation events.
- (3) A seismic disaster control mechanism based on the "dual compensation theory" was proposed. High-prestress NPR anchor cables were used to provide excavation stress compensation, while dual-sided roof cutting and unloading techniques were employed for mining space compensation. Field experiments demonstrated that the "dual compensation theory" and its related control technologies effectively reduced the energy level and frequency of seismic events, significantly improved the stability of roadway surrounding rock, and ensured safe and efficient mining operations. The remarkable results highlight the significant effectiveness of the proposed methods in preventing key stratum fracture-induced seismic events.

Declaration of Competing Interest

The authors declare that they have no known competing financial interests or personal relationships that could have appeared to influence the work reported in this paper.

Acknowledgments

This work was supported by the National Natural Science Foundation of China (Grant No. 52174096, 52304110); the Ordos Science & Technology Plan (Grant No. TD20240003); the Ordos science and Technology Bureau (Grant No. IMRI23005); the Ordos Science & Technology Plan (Grant No. YF20240021).

References

- [1] Wang Z B, Liu R F, Wang T T, et al. Energy Release Efficiency and Mechanisms of Mining-Induced High-Energy Earthquakes in China[J]. *Rock Mechanics and Rock Engineering*, 2025: 1-15.
- [2] Zou J, Zhang Q, Jiang Y, et al. Mechanism of hydraulic fracturing for controlling strong mining-induced earthquakes induced by coal mining[J]. *International Journal of Rock Mechanics and Mining Sciences*, 2024, 181: 105840.
- [3] Malinowska A A, Witkowski W T, Guzy A, et al. Mapping ground movements caused by mining-induced earthquakes applying satellite radar interferometry[J]. *Engineering Geology*, 2018, 246: 402-411.
- [4] Li Y, Fukuyama E, Yoshimitsu N. Mining-induced fault failure and coseismic slip based on numerical investigation[J]. *Bulletin of Engineering Geology and the Environment*, 2024, 83(10): 386.
- [5] Zhang Q, Zou J, Chi M, et al. Strong mining-induced earthquakes produced by the fracturing of key strata during deep coal mining[J]. *International Journal of Geomechanics*, 2024, 24(5): 04024080.
- [6] Kuang T, Li Z, Zhu W, et al. The impact of key strata movement on ground pressure behaviour in the Datong coalfield[J]. *International Journal of Rock Mechanics and Mining Sciences*, 2019, 119: 193-204.
- [7] Xia B, Jia J, Yu B, et al. Coupling effects of coal pillars of thick coal seams in large-space stopes and hard stratum on mine pressure[J]. *International Journal of Mining Science and Technology*, 2017, 27(6): 965-972.
- [8] Xiong Y, Kong D, Song G. Analysis of inclined length effect of roof fracture and overlying strata catastrophe in steeply inclined longwall face: a case study[J]. *Engineering Failure Analysis*, 2024, 160: 108243.
- [9] Dai X, Gao R, Du F, et al. Evolution and control of overburden fracture in extra-thick coal seam mining with hard roofs: ground grouting sealing and case study[J]. *Bulletin of Engineering Geology and the Environment*, 2024, 83(7): 262.
- [10] Zhou L, Li X, Peng Y, et al. Material point method with a strain-softening model to simulate roof strata movement induced by progressive longwall mining[J]. *International Journal of Rock Mechanics and Mining Sciences*, 2023, 170: 105508.

- [11] Liu Y, Cheng J, Jiao J, et al. Influences of the hard rock proportion coefficient on the evolution pattern and fractal characteristics of mining fractures in a composite roof[J]. *International Journal of Geomechanics*, 2024, 24(4): 04024038.
- [12] Deng G, Xie H, Gao M, et al. Fracture mechanisms of competent overburden under high stress conditions: A case study[J]. *Rock Mechanics and Rock Engineering*, 2023, 56(3): 1759-1777.
- [13] Wu F, Liu C, Yang J. Mode of overlying rock roofing structure in large mining height coal face and analysis of support resistance[J]. *Journal of Central South University*, 2016, 23(12): 3262-3272.
- [14] Cheng G, Ma T, Tang C, et al. A zoning model for coal mining-induced strata movement based on microseismic monitoring[J]. *International Journal of Rock Mechanics and Mining Sciences*, 2017, 94: 123-138.
- [15] Ning J, Wang J, Jiang L, et al. Fracture analysis of double-layer hard and thick roof and the controlling effect on strata behavior: a case study[J]. *Engineering Failure Analysis*, 2017, 81: 117-134.
- [16] Li G, Wang X, Bai J, et al. Research on the failure mechanism and control technology of surrounding rock in gob-side entry driving under unstable overlying strata[J]. *Engineering Failure Analysis*, 2022, 138: 106361.
- [17] Li Z, Dou L, Cai W, et al. Investigation and analysis of the rock burst mechanism induced within fault-pillars[J]. *International Journal of Rock Mechanics and Mining Sciences*, 2014, 70: 192-200.
- [18] Kuang T, Li Z, Zhu W, et al. The impact of key strata movement on ground pressure behaviour in the Datong coalfield[J]. *International Journal of Rock Mechanics and Mining Sciences*, 2019, 119: 193-204.
- [19] Wang F, Xu J, Xie J. Effects of arch structure in unconsolidated layers on fracture and failure of overlying strata[J]. *International Journal of Rock Mechanics and Mining Sciences*, 2019, 114: 141-152.
- [20] Zhao Y, Wang S, Zou Z, et al. Instability characteristics of the cracked roof rock beam under shallow mining conditions[J]. *International Journal of Mining Science and Technology*, 2018, 28(3): 437-444.
- [21] He M, Wang Q. Excavation compensation method and key technology for surrounding rock control[J]. *Engineering Geology*, 2022, 307: 106784.
- [22] He M, Gong W, Wang J, et al. Development of a novel energy-absorbing bolt with extraordinarily large elongation and constant resistance[J]. *International Journal of Rock Mechanics and Mining Sciences*, 2014, 67: 29-42.
- [23] Wang Q, Xu S, Xin Z, et al. Mechanical properties and field application of constant resistance energy-absorbing anchor cable[J]. *Tunnelling and Underground Space Technology*, 2022, 125: 104526.
- [24] He M, Wang Q. Rock dynamics in deep mining[J]. *International Journal of Mining Science and Technology*, 2023, 33(9): 1065-1082.
- [25] Zhang J, He M, Yang G, et al. N00 method with double-sided roof cutting for protecting roadways and Surface

Strata[J]. Rock Mechanics and Rock Engineering, 2024, 57(3): 1629-1651.

- [26] Yang G, Yang X, He M, et al. Experimental and numerical investigations of goaf roof failure and bulking characteristics based on gob-side entry retaining by roof cutting[J]. Engineering Failure Analysis, 2024, 158: 108000.
- [27] He M, Sui Q, Li M, et al. Compensation excavation method control for large deformation disaster of mountain soft rock tunnel[J]. International Journal of Mining Science and Technology, 2022, 32(5): 951-963.
- [28] Hu J, He M, Li H, et al. Rockburst disaster control using the excavation compensation method (ECM): A case study in the Qinling Water Conveyance Tunnel[J]. Engineering, 2024, 34: 154-163.